Available online at www.sciencedirect.com

SCIENCE DIRECT

Powder Technology 156 (2005) 177 – 194

POWDER TECHNOLOGY

www.elsevier.com/locate/powtec

Modeling and control of HVOF thermal spray processing of WC–Co coatings

Mingheng Li, Dan Shi, Panagiotis D. Christofides*

Department of Chemical Engineering, University of California, Los Angeles, CA 90095-1592, United States

Available online 21 July 2005

Abstract

This work focuses on the modeling and feedback control of the high velocity oxygen fuel (HVOF) thermal spray processing of WC–Co coatings. A first-principles-based process model is proposed to explore the fluid dynamics and particle inflight behavior in the HVOF flow field. Rule-based stochastic simulation, which encapsulates the main features involved in the deposition process, is used to capture the evolution of coating microstructure. The multiscale modeling of HVOF thermal spray process reveals that the velocity and melting degree of particles at the point of impact on the substrate play a very important role in the formation of coating microstructure, which in turn, can be almost independently controlled by pressure and fuel/oxygen ratio, respectively. Based on model predictions and available experimental observations, the control problem is formulated as the one of regulating volume-based averages of particle velocity and melting degree at impact on the substrate by manipulating the feed rate of air, oxygen and fuel at the entrance of the thermal spray gun, through which the pressure and oxygen/fuel ratio can be independently adjusted. A feedback control system is then developed and applied to a detailed mathematical model of the process. Closed-loop simulations show that the feedback controller is effective in driving the controlled outputs to the desired set-point values and also robust with respect to various kinds of disturbances in the operating environment.
© 2005 Elsevier B.V. All rights reserved.

Keywords: High velocity oxygen fuel (HVOF) thermal spray; Coatings; Microstructure; Process modeling; Particle size distribution; Feedback control

1. Introduction

The high velocity oxygen fuel (HVOF) thermal spray process is a process of particulate deposition in which fine powder particles, normally in the size range 5 to 65 μm, are heated and accelerated in a reacting gas stream and subsequently hit the substrate in a molten or semi-molten state, forming a thin layer of coating as a result of the solidification and sintering of the sprayed particles. Featured with very high particle velocities and relatively low particle temperatures as compared to those in the plasma spray process, the HVOF thermal spray provides a highly efficient way to coating processing in order to extend product life, increase performance and reduce production and maintenance costs. Nowadays, the HVOF thermal spray has carved out a special niche in the thermal spray industry, particularly in the fabrication of nanostructured coatings, because the particle vaporization or overheating is avoided during flight and the nanocrystalline structure of powder particles can be preserved [1].

In order to reduce coating variability in industrial HVOF thermal spray processes, it is important to implement excellent real-time process diagnosis and control which could suppress the influence of external disturbances. Despite the recent progress on the modeling of various phenomena that affect droplet motion, deposition, solidification and microstructure development in HVOF thermal spray processes [2–8], at this stage, there exists no systematic framework for integrated on-line diagnosis and control of the HVOF thermal spray process which will be capable of achieving precise regulation of the microstructure and ultimate mechanical and thermal properties of the sprayed coatings. In addition, incorporation of advanced real-time diagnosis and control schemes into thermal spray processes is expected to reduce operational cost and

* Corresponding author. Tel.: +1 310 794 1015; fax: +1 310 206 4107.
E-mail address: pdc@seas.ucla.edu (P.D. Christofides).

0032-5910/$ - see front matter © 2005 Elsevier B.V. All rights reserved.
doi:10.1016/j.powtec.2005.04.011

environmental impact, and allow depositing nanostructured and complex (multi-material) coatings with very low variability. Since the application of optimization and control techniques to spray casting processes has been reported to lead to significant improvements in their operation and performance (e.g., [9,10]), it is important to develop real-time computer control systems for thermal spray processes by integrating fundamental models that accurately describe the inherent relationships between the coating microstructure and the processing parameters with on-line state-of-the-art diagnostic techniques and control algorithms. Recent efforts in this direction have mainly focused on diagnostics and control of the plasma thermal spray process (see [11]); the reader may also refer to [12] for a discussion of various process optimization and control issues.

Motivated by the above, in a previous work [13,14], we performed a comprehensive control-relevant parametric analysis and proposed a novel formulation of the control problem that accounts for the important effect of powder size distribution (see [15–20] and the book [21] for nonlinear control of particulate processes accounting for powder size distribution) for a thermal spray process in which air is used as oxidant and propane is used as fuel gas. Based on this formulation of the control problem, we recently developed a practical control system for an industrial HVOF thermal spray process—the Metco Diamond Jet hybrid gun, manufactured by Sulzer Metco, Westbury, New York [22]. In continuation of the previous work, the HVOF thermal spray processing of WC–Co coatings is studied in this paper. A first-principles-based process model is proposed to explore the fluid and particle dynamics in the HVOF flow field. Rule-based stochastic simulation, which encapsulates the main features involved in the deposition process, is used to describe the evolution of coating microstructure. Based on modeling predictions and available experimental studies, which reveal that particle velocity and melting degree play a very important role in the formation of coating microstructure and can be almost independently controlled by pressure and oxygen/fuel ratio, respectively, the control problem is formulated as the one of regulating volume-based averages of particle velocity and melting degree at the point of impact on substrate by manipulating the gas flow rate of air, oxygen and fuel at the entrance of the thermal spray gun, through which the pressure and oxygen/fuel ratio can be independently adjusted. A feedback control system is then developed and applied to a detailed mathematical model of the process. Closed-loop simulations show that the feedback controller is effective in driving the controlled outputs to the desired set-point values and also robust with respect to various kinds of disturbances in the operating environment.

2. Modeling of thermal and flow fields

2.1. Process description and modeling procedure

Fig. 1 shows a schematic diagram of the Diamond Jet hybrid gun. The fuel gases (typically propylene or hydrogen), which are thoroughly mixed with oxygen through a siphon system, are fed to the air cap, where they react to produce high temperature combustion gases. The exhaust gases, together with the air injected from the annular inlet orifice, expand through the nozzle to reach supersonic velocity. The air cap is water-cooled to prevent from being melted. The powder particles are injected from the central inlet hole using nitrogen as the carrier gas. Consequently, rapid momentum and heat transfer between the gas and the powder particles leads to acceleration and heating of the powder particles. The molten or semi-molten particles exit the air cap and move towards the substrate. The particles hit the substrate with very high velocities, cool and solidify, forming a thin layer of dense and hard coating.

Roughly speaking, there are three major physicochemical processes involved in the macroscopic HVOF flow field: transformation of chemical energy into thermal energy by the combustion of the fuel, conversion of thermal energy into kinetic energy of the burning gases by passing through the nozzle and transfer of momentum and heat from the gases to the powder particles. To simplify the analysis, the process model used in this paper is based on the one-way coupling assumption, i.e., the existence of particles has a minimal influence on the gas dynamics while the particle in-flight behavior is dependent on the gas thermal/flow field. This assumption is reasonably accurate because the particle loading in the HVOF thermal spray process is typically less than 4% [23]. In addition, in

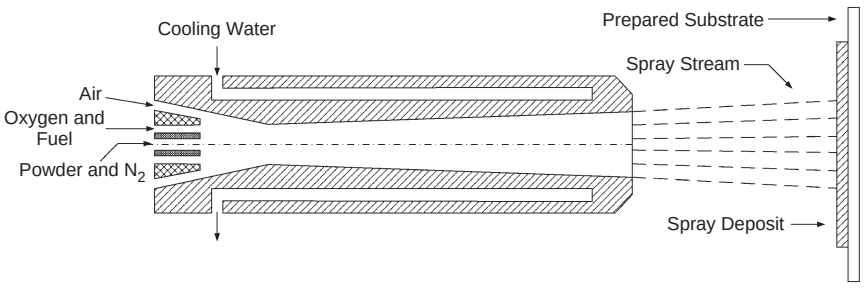

Fig. 1. A schematic of the Diamond Jet hybrid HVOF thermal spray process.

order to make the reactive flow process much easier to handle, a commonly used assumption that the chemical reaction rate is much faster than the time-scale associated with the gas dynamics [24], is employed here. Based on this, the assumptions of instantaneous equilibrium at the entrance of the HVOF gun and frozen isentropic flow during passage through the nozzle are made. These assumptions were initially proposed and justified by Swank et al. [25] through comparison of numerical simulations and experimental results, and later also suggested by Cheng et al. [24] and substantiated by the simulation results of Li et al. [22]. Regarding the role of the air stream, it was assumed that all the oxygen coming from the air participates in the reaction [26–28]. Gourlaouen et al. [27] pointed out that the airflow mixing with the oxygen/propylene mixture is more effective in the currently used Diamond Jet hybrid gun (which is the process under consideration in this work) than the previous Diamond Jet gun, as implied by the "water-cooled" (not "air-cooled-only") nozzle. Other assumptions in the modeling include: (1) all the gases obey ideal gas law; (2) the combustion gases behave like a perfect gas during isentropic compression and expansion, and the specific heat ratio is nearly constant; and (3) the friction and cooling water effects along the nozzle and barrel are negligible so that laws of isentropic flow of compressible fluids apply.

Because the flow is choked at the throat of the nozzle, the convergent part of the air cap and the divergent one can be solved separately [28]. The modeling procedure that is followed in the simulation is based on the sequential modular method, as shown in Fig. 2. Specifically, given the mass flow rates of each stream (fuel, oxygen, air and carrier gas) and a postulated combustion pressure, the temperature and gas composition at the entrance of the nozzle is calculated using an instantaneous equilibrium model, and the nozzle flow is then solved using standard isentropic compressible flow relationships. Subsequently, the total mass flow rate at the throat of the nozzle is calculated and compared with the one at the entrance. The combustion pressure is then adjusted using the shooting method, until the discrepancy between the calculated and specified values of the total mass flow rate falls below a pre-specified tolerance. After the gas properties at the nozzle throat are determined, the divergent part is solved using isentropic flow relationships. The external thermal/flow field in the free jet is described by empirical formulas. After the gas dynamics is determined, the momentum transfer and heat transfer equations are used to solve the particle trajectories and temperature histories.

2.2. Governing equations

In the combustion chamber (convergent section of the nozzle), the exothermic fuel/oxygen reaction increases the gas temperature to around 3000 K, at which several components in the product mixture, including O_2 and H_2O, partially dissociate into a number of light species such as H, O, OH, etc. because of strong thermal atomic vibration. An equilibrium chemistry model shown below is used to describe the combustion process:

$$\begin{aligned}\varphi C_3H_6 + 4.5O_2 + w[N_2 + 1/78Ar] + zN_2 \Rightarrow & \xi_1 CO \\ & + \xi_2 CO_2 + \xi_3 H + \xi_4 H_2 + \xi_5 H_2O + \xi_6 O + \xi_7 OH \\ & + \xi_8 O_2 + \xi_9 C_3H_6 + \xi_{10} Ar + \xi_{11} N_2 + \xi_{12} NO \end{aligned} \quad (1)$$

where φ is the so-called equivalence ratio, or the ratio of fuel/oxygen to its stoichiometric condition value, w and z the coefficient of nitrogen coming from the air and the carrier gas, respectively, and ξ_1–ξ_{12} the coefficients of the combustion products. It is assumed that the above reaction is complete as soon as the gases enter the chamber. The composition and temperature at equilibrium for the above system can be uniquely determined by minimizing the Gibbs energy of the whole system based on the information of initial gas composition and chamber pressure. For the detailed solution methodology, the reader may refer to [22,29], where it is shown that under normal operating conditions, propylene does not exist in the product mixture.

For an ideal gas under adiabatic and isentropic conditions, the gas temperature, pressure and density are

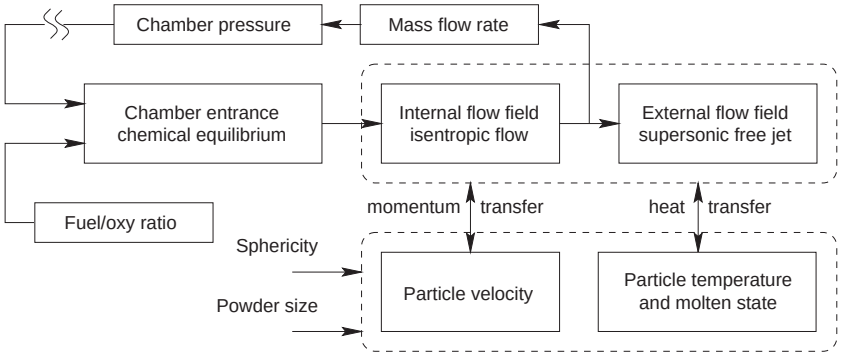

Fig. 2. Modeling procedure of the gas and particle field.

related to the stagnation properties by the following equations:

$$\frac{T_0}{T} = 1 + \frac{1}{2}(\gamma - 1)\mathbf{M}^2$$

$$\frac{P_0}{P} = \left[1 + \frac{1}{2}(\gamma - 1)\mathbf{M}^2\right]^{\gamma/(\gamma-1)}$$

$$\frac{\rho_0}{\rho} = \left[1 + \frac{1}{2}(\gamma - 1)\mathbf{M}^2\right]^{1/(\gamma-1)} \quad (2)$$

where T is the temperature, P the pressure, ρ the density and γ the specific heat ratio. Subscript 0 stands for the stagnation condition (a reference condition at which the velocity is zero). The gas velocity is related to the Mach number (**M**), pressure, and density by:

$$v = \mathbf{M}\sqrt{\gamma \mathbf{P}/\boldsymbol{\rho}} \quad (3)$$

and the Mach number is a function of the cross sectional area perpendicular to the flow direction (A):

$$\frac{A_2}{A_1} = \frac{\mathbf{M}_1}{\mathbf{M}_2}\left\{\frac{1 + [(\gamma - 1)/2]\mathbf{M}_2^2}{1 + [(\gamma - 1)/2]\mathbf{M}_1^2}\right\}^{(\gamma+1)/2(\gamma-1)} \quad (4)$$

Eqs. (2)–(4) set up a relationship of gas properties (pressure, density, temperature, velocity and Mach number) between two positions in the nozzle. Since as described above, the flow is choked at the throat area, the gas flow rate using the critical conditions can be determined by:

$$\dot{m}_g = \rho_t v_t A_t = \frac{P_0}{\sqrt{T_0}} A_t \left[\frac{\gamma \bar{M}_{pr}}{R}\left(\frac{2}{\gamma + 1}\right)^{(\gamma+1)/(\gamma-1)}\right]^{1/2} \quad (5)$$

where $\bar{M}_{pr}$ is the average molecular weight of the gas mixture. When the solution is convergent, the calculated mass flow rate should match the specified mass flow rate at the entrance of the gun. When the gas properties at the throat of the nozzle are determined, the entire nozzle can be readily solved using Eqs. (2)–(4). Regarding the supersonic free jet in the external flow field, it is quite complex and is modeled by taking advantage of the experimentally measured data of supersonic free jets [25,30–33]. The data is correlated using formulas of the following form [34]:

$$\overline{gp} = 1 - \exp\left(\frac{\alpha}{1 - \bar{x}/\beta}\right) \quad (6)$$

where $\overline{gp}$ refers to normalized gas properties (v/v_e, $(T-T_a)/(T_e-T_a)$ and $(\rho-\rho_a)/(\rho_e-\rho_a)$, where subscripts a and e stand for atmospheric condition and nozzle exit condition, respectively) and $\bar{x}$ is the normalized axial distance from the exit of the nozzle ($\bar{x}=x/D$, where D is the diameter of the nozzle exit). Piecewise constant expression for α and β are used to make the curve smooth. The results are shown in Fig. 3. It can be seen that the correlation formulas fit

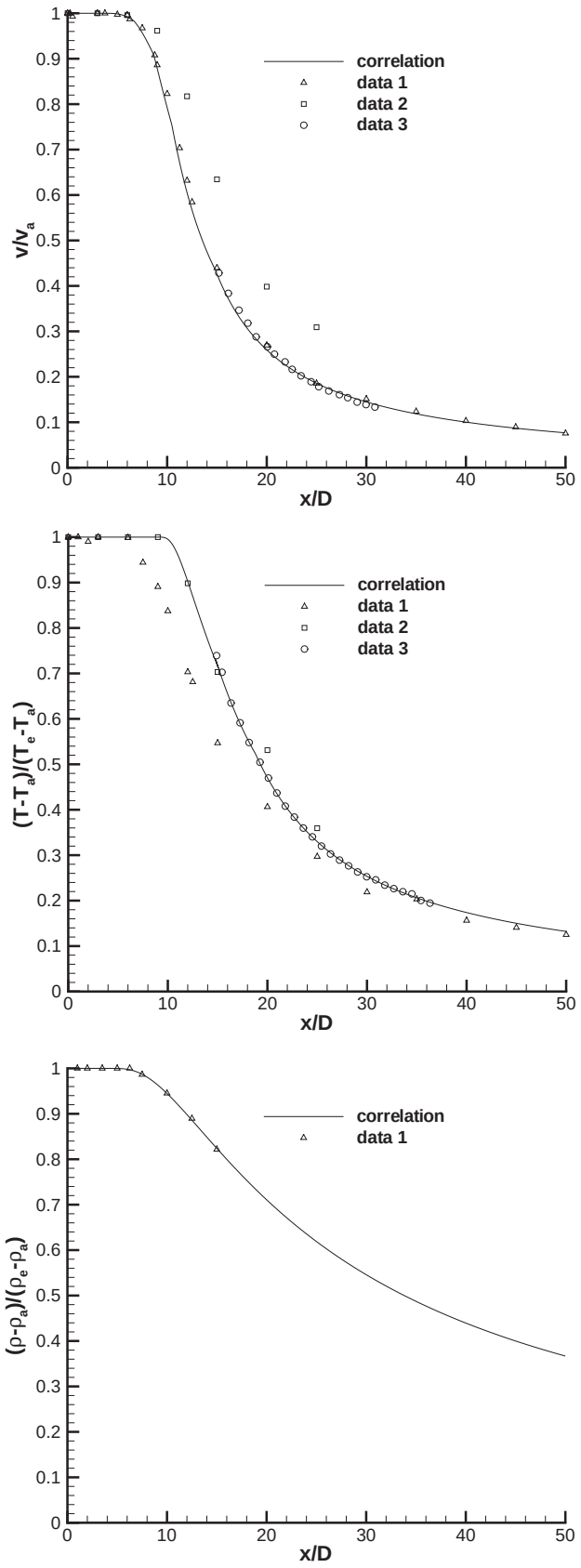

Fig. 3. Correlation of gas velocity, temperature and density in the supersonic free jet. Data 1—Mach number=1.8, ρ_e/ρ_{air}=3.7 [30,31], data 2—Mach number=2.0 [32], data 3—Mach number=2.0, ρ_e/ρ_{air}=7–8 [25,33].

well the experimental data obtained from a similar HVOF thermal spray process [25,33].

The particle trajectories and temperature histories in the gas field are computed by the following momentum and heat transfer equations:

$$m_p \frac{dv_p}{dt} = \frac{1}{2} C_D \rho_g A_p (v_g - v_p)|v_g - v_p|$$

$$\frac{dx_p}{dt} = v_p$$

$$m_p c_{p_p} \frac{dT_p}{dt} = \begin{cases} hA'_p(T_g - T_p) + S_h, & (T_p \neq T_m) \\ 0, & (T_p = T_m) \end{cases}$$

$$\Delta H_m m_p \frac{df_p}{dt} = \begin{cases} hA'_p(T_g - T_p) + S_h, & (T_p = T_m) \\ 0, & (T_p \neq T_m) \end{cases} \quad (7)$$

where m_p is the mass of the particle, t the time, v_p the axial velocity of the particle, A_p the projected area of the particle on the plane perpendicular to the flow direction, ρ_g the density of the gas, C_D the drag coefficient, x_p the position of the particle, T_p the temperature of the particle, A'_p the surface area of the particle, T_m the melting point of the particle, ΔH_m the enthalpy of melting, f_p the mass fraction of melted part in the particle ($0 \leq f_p \leq 1$) and S_h the source term including heat transfer due to radiation ($\varepsilon\sigma A'_p(T_g^4 - T_p^4)$) and oxidation. The heat transfer coefficient h is computed by the Ranz-Marshall empirical equation [35]:

$$h = \frac{\lambda_g}{d_p}\left[2 + 0.6 Re^{\frac{1}{2}} Pr^{\frac{1}{3}}\right] \quad (8)$$

where the local Reynolds number (Re) for this two phase flow problem is defined based on the relative velocity $Re = d_p|v_g - v_p|\rho_g/\eta_g$, and the Prandtl number (Pr) is calculated by $Pr = c_{p_g}\eta_g/\lambda_g$. The above equations describing particle velocity, position, temperature and degree of particle melting are solved by 4th order Runge–Kutta method. In all the mathematical formulas, the thermodynamic and transport properties of each species and product mixture are calculated using formulas provided in [29].

Remark. In the HVOF thermal spray processing of particles consisting of carbides with binding metals, such as the WC–Co powders used in this work, only the latter may experience a molten state [36] because the gas temperature in a conventional HVOF thermal spray process is not high enough to melt the carbides, whose melting point is very high (2870 °C for tungsten carbide). In such a case, the heating equation Eq. (7) should be modified such that only the fusion of metals might occur in the gas thermal field. In the following text, the melting degree of particles stands for the one of the binder instead of the whole particulate phase.

3. Modeling of coating microstructure

A thermally sprayed coating consists of lamellar splats interspersed with pores. The splats, which are the fundamental building blocks of the coating, are formed by the impact, deformation, spreading and solidification of individual droplets, and the pores are formed by the interaction of the droplets and the previously deposited coating surface. In the particle deposition and coating microstructure formation model, it is assumed that the coating growth process is a sequence of independent discrete events of each individual particle hitting on the previously formed coating layer. In the simulation, the size of each particle is chosen randomly from a lognormally-distributed particle size function [37], and its velocity, temperature and melting ratio of this particle at the point of impact on the substrate are calculated using the particle dynamics model developed in the previous section. The hitting point of the particle on the substrate is determined by two uniformly distributed random numbers. The particle then hits the substrate, forms a splat, and is then added to the previously formed coating surface based on certain rules, until the coating thickness reaches its specified value. Specifically, the powder size distribution function is of the following form [37]:

$$f(d_p) = \frac{1}{\sqrt{2\pi}\sigma d_p} \exp\left[-\frac{(\ln d_p - \mu)^2}{2\sigma^2}\right] \quad (9)$$

where $f(d_p)$ is the size distribution function, μ and σ^2 are two dimensionless parameters corresponding to the mean and the variance of $\ln d_p$, which obeys the normal distribution. For particles that are lognormally distributed, μ and σ can be determined by the following formulas [13]:

$$\mu = \ln\sqrt[3]{d_{10}d_{50}d_{90}} - 1.831\left(\ln\sqrt{\frac{d_{90}}{d_{10}}}\right)^2$$

$$\sigma = 0.781 \ln\sqrt{\frac{d_{90}}{d_{10}}} \quad (10)$$

where d_{10}, d_{50} and d_{90} are three characteristic diameters that can be determined experimentally [38].

Furthermore, it is assumed that the particle deformation follows the law of Madejski [39], i.e., the droplet becomes a thin cylinder as a result of deformation and the flattening ratio ξ follows the analysis of Madejski [39]:

$$\xi = \frac{D_s}{d_p} = \frac{2}{d_p}\sqrt{\frac{A_s}{\pi}} \quad (11)$$

where D_s and A_s are the estimated diameter and area of the splat, respectively, and d_p is the particle diameter prior to

impact. Note the volume of a cylinder is $(1/4)\pi D_s^2 H_s$, where H_s is the height and, D_s and H_s can be calculated by:

$$\begin{cases} D_s & = \xi d_p \\ H_s & = \dfrac{2d_p}{3\xi^2} \end{cases} \tag{12}$$

The analysis of Madejski shows that ξ depends on several dimensionless parameters characterizing the impact and spreading processes, including: the Reynolds number, which represents the viscous dissipation of the inertia forces, the Weber number, which quantifies the conversion of the kinetic energy into surface energy, and the Peclet number, which expresses the freezing rate. In this paper, a simplified formula of ξ is used, which takes the following form [39]:

$$\xi = 1.2941 Re^{0.2} \tag{13}$$

Note that not all particles can be fully melted in the HVOF thermal spray process, for a partially melted particle, it is assumed in this paper that the unmelted part will form a hemisphere with the equivalent volume and the melted part will form a ring around this hemisphere, whose flattening ratio can be calculated using the same formula.

Finally, depending on the physical state of the spray particle and the condition of the previously deposited coating surface at the hitting point, several different events may occur as a particle hits the substrate. These events are governed by certain rules shown below.

1. When a particle hits the substrate, the melted part usually fits on the surface as much as possible.
2. If the unmelted part of a partially melted particle hits at the point of the previously deposited layer that is formed by an unmelted particle, it will bounce off, and a hole will be formed in the center of the disk. Otherwise, it will attach on the coating surface as a hemisphere and macro-size pores may form under the hemisphere.
3. If the splat comes to a vertical drop during spreading, the ratio of the splat that has not been settled down will be calculated. The splat may either cover a gap or break (or cover the corner) at the step, depending on the ratio and the height of the step.
4. If the splat encounters a dead end, it will first fill the available space, and then flow over the outer surface if the volume of the splat is bigger than the available space.

Table 1
Baseline operating conditions

Gas	Propylene	Oxygen	Air	Nitrogen
Mass flow rate (10^{-3} kg/s)	2.596	6.495	8.727	0.280

Table 2
Calculated gas equilibrium composition under baseline conditions

Species	Coefficient	Species	Coefficient
CO	0.13431	OH	0.04198
CO_2	0.13796	O_2	0.04158
H	0.01468	C_3H_6	0
H_2	0.02753	Ar	0.00442
H_2O	0.21642	N_2	0.35118
O	0.01348	NO	0.01645

A detailed discussion of the rule-based stochastic modeling of coating microstructure was given in our previous work [8].

4. Open-loop simulation results and analysis

The gas phase dynamics under the baseline operating conditions (shown in Table 1) is solved numerically and the calculated gas equilibrium composition is listed in Table 2. It is shown that even under the fuel rich condition ($\varphi = 1.045$), propylene does not show up in the combustion product mixture. Instead, the fraction of oxygen (O plus O_2) is about 5.5%. Due to the existence of oxygen in the internal flow field and the entrainment of air in the external flow field, the powder particles may be oxidized, and their temperatures can be increased due to the exothermic oxidation reaction.

The calculated gas properties in the internal flow field and profiles of gas velocity, temperature and density are shown in Table 3 and Fig. 4. The gas properties at the entrance of the gun is calculated based on the equilibrium model. It is shown that the highest temperature of propylene combustion under the baseline condition is a little higher than 3100 K and a high pressure of 6.7 bar is maintained in the chamber. However, as the combustion gases pass through the convergent divergent nozzle, the thermal energy is partially converted to kinetic energy. As a consequence, the gas velocity increases from subsonic to supersonic and both pressure and temperature decrease. In particular, the pressure at the exit of the gun is less than one atmosphere, which implies the flow outside of the gun will be overexpanded. This conclusion has been validated by experimental measurements [40].

The calculated gas thermodynamic and transport properties in the internal and external flow fields under the baseline conditions are shown in Table 4. As the gas

Table 3
Calculated gas properties in the internal flow field

Parameter	Entrance	Throat	Exit
Pressure (bar)	6.72	3.80	0.62
Temperature (K)	3127	2811	2006
Velocity (m/s)	172	1040	1946
Density (kg/m^3)	0.69	0.43	0.10
Mach number	0.16	1.00	2.21

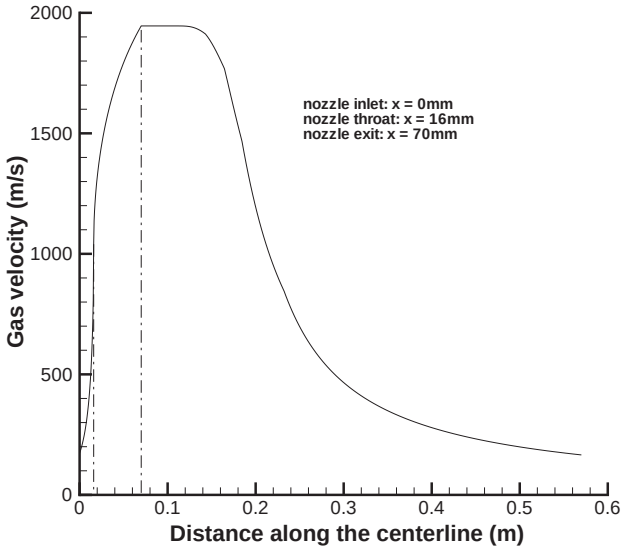

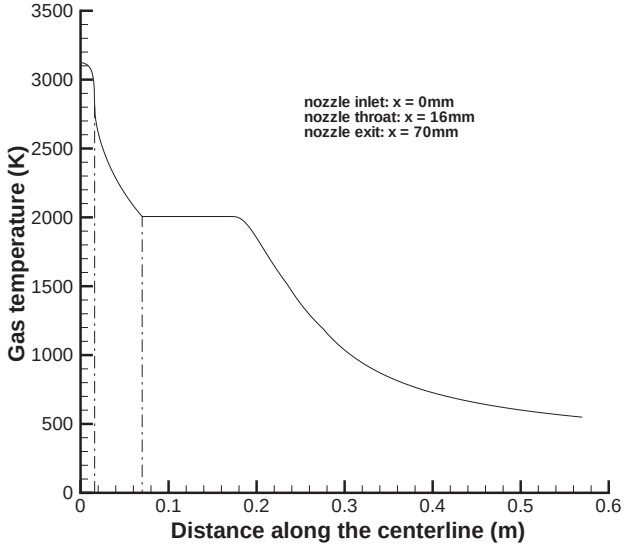

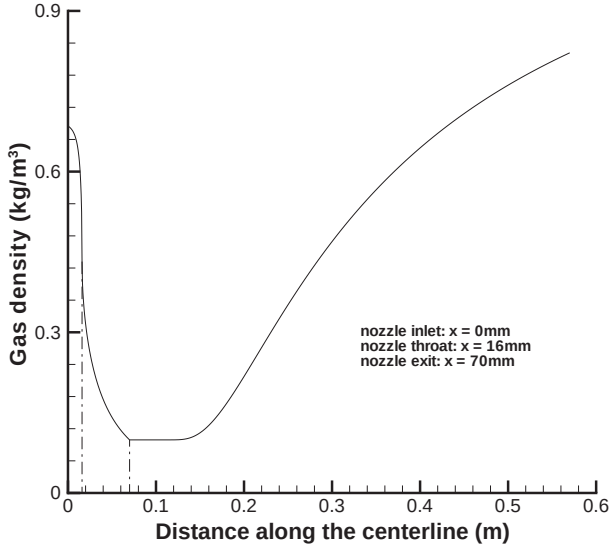

Fig. 4. Profiles of gas velocity, temperature and density along the centerline.

Table 4
Calculated gas thermodynamic and transport properties in the internal and external flow fields under the baseline operating conditions

Heat capacity, $\bar{c}_{p_g}$ (10^3 J/kg K)	1.4–1.7
Viscosity, $\bar{\eta}_g$ (10^{-5} kg/m/s)	4.5–9.4
Thermal conductivity, $\bar{\lambda}_g$ (W/m K)	0.09–0.23
Prandtl number, Pr	0.68–0.74
Isentropic ratio, γ	1.23–1.28

temperature decreases, the gas heat capacity, viscosity and thermal conductivity increase. As a result, the Prandtl number is almost constant (about 0.7). It should be noted that the isentropic ratio of the exhaust gas mixture is about 1.25, which is less than that of the air (about 1.4).

Due to the one dimensional model and the frozen flow assumption, the gas temperature is the highest at the chamber entrance and decreases monotonically in the axial direction. However, the gas temperature in the centerline usually increases sharply and then decreases because of the carrier gas (see, e.g., [2,41]). Although this stage is short, it plays an important role in particle heating because the particle residence time is relatively long in this region. To reasonably predict the particle temperature, we assume that the gas temperature increases linearly in the entire convergent part of the nozzle, from room temperature at the nozzle entrance to the calculated throat temperature at the nozzle throat. The resulting profiles of particle velocity, temperature and melting ratio are shown in Fig. 5. It can be seen that particles of small sizes may reach very high velocities during flight, however, their velocities drop more sharply than those of larger particles because of their smaller momentum inertias. Furthermore, they may be heated to the melting point in a short time and be fully melted during flight, however, they may eventually be in a coexistence state of liquid and solid or even in a solid state after a long enough distance. Smaller particles tend to change their temperatures more easily because of their smaller thermal inertias. For particles of large sizes, however, the periods for acceleration and heating are both longer, and the velocity (or temperature) profile becomes nearly flat as it approaches the same velocity (or temperature) of the gas. In addition, their temperature may not reach the melting point, and therefore, they remain in solid state during the entire flight. However, particles of medium sizes may become partially melted during flight.

It is interesting to observe that for large particles ($d_p \approx 20$ μm in this case), the particle velocity profile becomes almost flat after an acceleration stage, where $v_p \ll v_g$ holds. In order to find out the key factors for particle acceleration, we made the following analysis. Note that since $Re = d_p|v_g - v_p|\rho_g/\eta_g$, the first equation of the particle motion can be written as:

$$\frac{dv_p}{dt} = \frac{3\eta_g C_D Re}{4\rho_p d_p^2}\left(v_g - v_p\right) \tag{14}$$

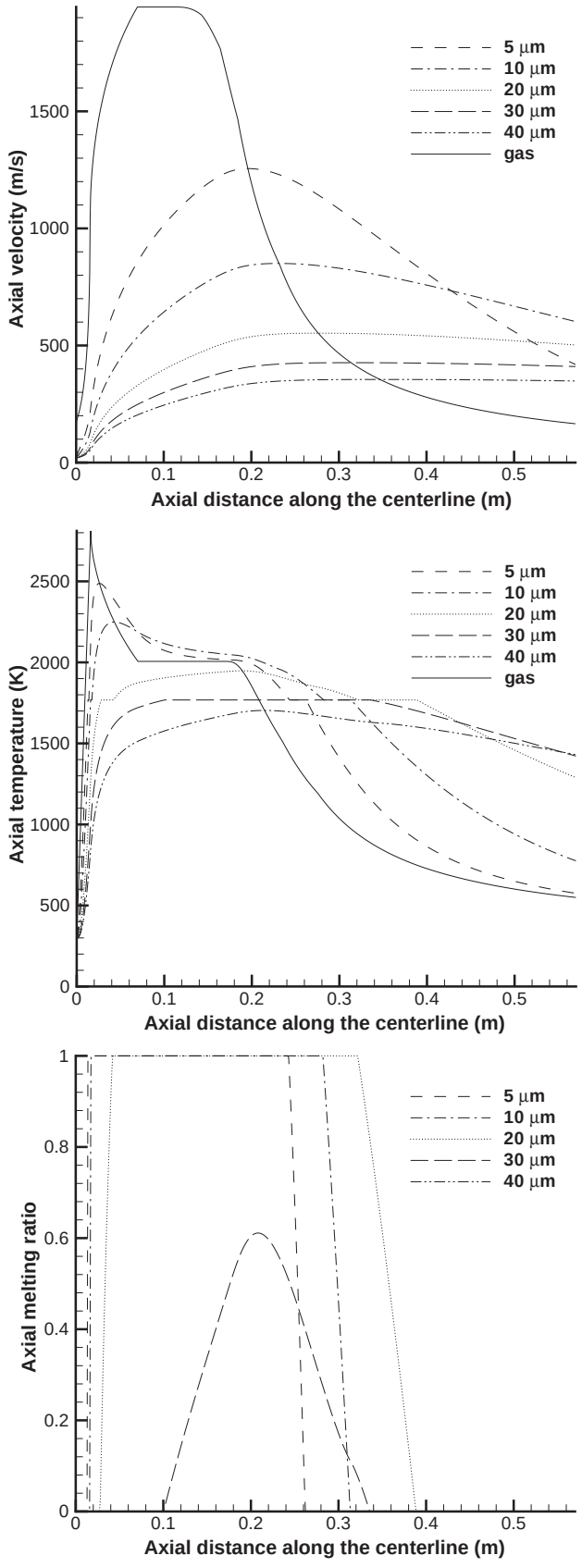

Fig. 5. Profiles of particle velocity, temperature and degree of melting along the centerline.

Dividing the first subequation by the second one in Eq. (7), one can derive

$$\frac{dv_p^2}{dx_p} = \frac{3\eta_g C_D Re}{2\rho_p d_p^2}\left(v_g - v_p\right) \tag{15}$$

Because the maximum velocity that the particles can achieve (especially for large particles) in the HVOF flow field is mainly decided by the initial acceleration stage when $v_p \ll v_g$ holds (this is because when the particle velocity approaches the gas velocity, the drag force term becomes small and the particle velocity profile becomes almost flat). Approximating $(v_g - v_p)$ by v_g, Eq. (15) can be analytically solved to yield:

$$v_p = \sqrt{\int_0^{x_p} \frac{3\eta_g C_D Re}{2\rho_p d_p^2} v_g dx_p + v_{p_0}^2} \tag{16}$$

For particles in the HVOF gas field, the Reynolds number based on the relative velocity is typically less than 10^3, and C_D can be approximately calculated by $18.5/Re^{0.6}$ [35]. Therefore,

$$v_p = \sqrt{\int_0^{x_p} \frac{28 v_g^{1.4} \rho_g^{0.4} \eta_g^{0.4}}{\rho_p d_p^{1.6}} dx_p + v_{p_0}^2} \tag{17}$$

If one checks the magnitude of the first term and the second one under the square root in Eq. (17) it can be found that $v_{p_0}^2$ can be almost neglected. The following parameters are used to estimate these terms: $v_g = 10^3$ m/s, $\rho_g = 10^{-1}$ kg/m^3, $\eta_g = 10^{-5}$ kg/m/s, $\rho_p = 10^4$ kg/m^3, $d_p = 10^{-5}$ m, $x_p = 10^{-2}$ m, it can be easily figured out that $\int_0^{x_p} \left(28 v_g^{1.4} \rho_g^{0.4} \eta_g^{0.4}\right) / \left(\rho_p d_p^{1.6}\right) dx_p = 10^5 \mathrm{m}^2/\mathrm{s}^2$. If $v_{p_0} = 30$ m/s, $v_{p_0}^2$ will be just 1% of the aforementioned integral. Therefore, Eq. (18) can be further simplified to be

$$v_p = \sqrt{\int_0^{x_p} \frac{28 v_g^{1.4} \rho_g^{0.4} \eta_g^{0.4}}{\rho_p d_p^{1.6}} dx_p} \tag{18}$$

The above equation shows that a very short flight distance of the particles will compensate for the effect of the change in particle injection velocity, and therefore, the latter has a negligible effect on particle final velocity. However, since $\rho_g v_g^2 = \gamma \mathbf{M}^2 P$, it can be concluded that a high chamber pressure, a high gas velocity and a high gas viscosity will lead to an increase in particle velocity. Furthermore, the larger the particle size and the higher the particle density, the lower the maximum velocity the particle can achieve.

Similar analysis can be made on the particle heating equation. Note in Eq. (7) we used a first order ODE to describe particle heating, which holds only when the Biot number (the ratio of thermal internal resistance to surface

film resistance) is less than 0.1 [42]. This can be verified by the following analysis:

$$\mathrm{Bi} = \frac{hd_\mathrm{p}/6}{\lambda_\mathrm{p}} = \frac{Nu\lambda_\mathrm{g}/6}{\lambda_\mathrm{p}} \tag{19}$$

For tungsten carbide, $\lambda_\mathrm{p}=10^{1\sim2}$ W/m K, since $Nu=10^{0\sim1}$, $\lambda_\mathrm{g}=10^{-(1\sim2)}$ W/m K, the Biot number is much less than 0.1. In addition, the ratio of heat transfer due to convection to that due to radiation can be calculated by:

$$\frac{J_\mathrm{cov}}{J_\mathrm{rad}} = \frac{hA'_\mathrm{p}\left(T_\mathrm{g}-T_\mathrm{p}\right)}{\varepsilon\sigma A'_\mathrm{p}\left(T_\mathrm{g}^4-T_\mathrm{p}^4\right)} = \frac{Nu\lambda_\mathrm{g}}{d_\mathrm{p}\varepsilon\sigma\left(T_\mathrm{g}^2+T_\mathrm{p}^2\right)\left(T_\mathrm{g}+T_\mathrm{p}\right)} \tag{20}$$

Setting $Nu=10^{0\sim1}$, $\lambda_\mathrm{g}=10^{-(1\sim2)}$ W/m K, $d_\mathrm{p}=10^{-5}$ m, $T_\mathrm{g}=10^3$ K, $T_\mathrm{p}=10^3$ K, $\varepsilon=0.4$, $\sigma=5.67\times10^{-8}$ W/m^2 K^4, then one can figure out $J_\mathrm{cov}/J_\mathrm{rad}\approx10^2$, which shows radiation only accounts for no more than several percent of the total heat flux. If ignoring the particle melting behavior, one can derive that

$$\frac{\mathrm{d}T_\mathrm{p}}{\mathrm{d}x} = \frac{6h\left(T_\mathrm{g}-T_\mathrm{p}\right)}{d_\mathrm{p}\rho_\mathrm{p}c_{\mathrm{p}_\mathrm{p}}v_\mathrm{p}} \tag{21}$$

and

$$\frac{\mathrm{d}T_\mathrm{p}}{\mathrm{d}v_\mathrm{p}} = \frac{8\lambda_\mathrm{g}Nu\left(T_\mathrm{g}-T_\mathrm{p}\right)}{c_{\mathrm{p}_\mathrm{p}}\eta_\mathrm{g}C_\mathrm{D}Re\left(v_\mathrm{g}-v_\mathrm{p}\right)} \tag{22}$$

Although $T_\mathrm{p}\ll T_\mathrm{g}$ cannot be guaranteed, it can still be derived from the above equation that for large particles, the gas temperature can be increased by increasing the gas temperature or decreasing the particle velocity (or increase the particle residence time in the hot region). It can also be seen that the larger the particle size and the higher the particle density and heat capacity, the lower the highest particle temperature that can be achieved. Furthermore, $v_\mathrm{p}/T_\mathrm{p}$ can be increased by increasing $v_\mathrm{g}/T_\mathrm{g}$ and decreased by decreasing $v_\mathrm{g}/T_\mathrm{g}$, which can be used to regulate the relative magnitude of the particle velocity and temperature. Note that since the gas velocity is typically low in the convergent part of the nozzle, the particle heating can be significantly improved if the centerline gas temperature in this region is maintained at high levels.

To further understand the behavior of particles in the HVOF process, we also plotted the velocity, temperature and melting ratio at the 8 in. (0.203 m) standoff (default spray distance) as a function of particle size, shown in Fig. 6 (note that the configuration of each figure may vary with different spray distances). It is shown that particles in the size range 4–38 μm hit the substrate in a semi-molten state (where both liquid and solid coexist). Other particles, either smaller or larger, are in a solid

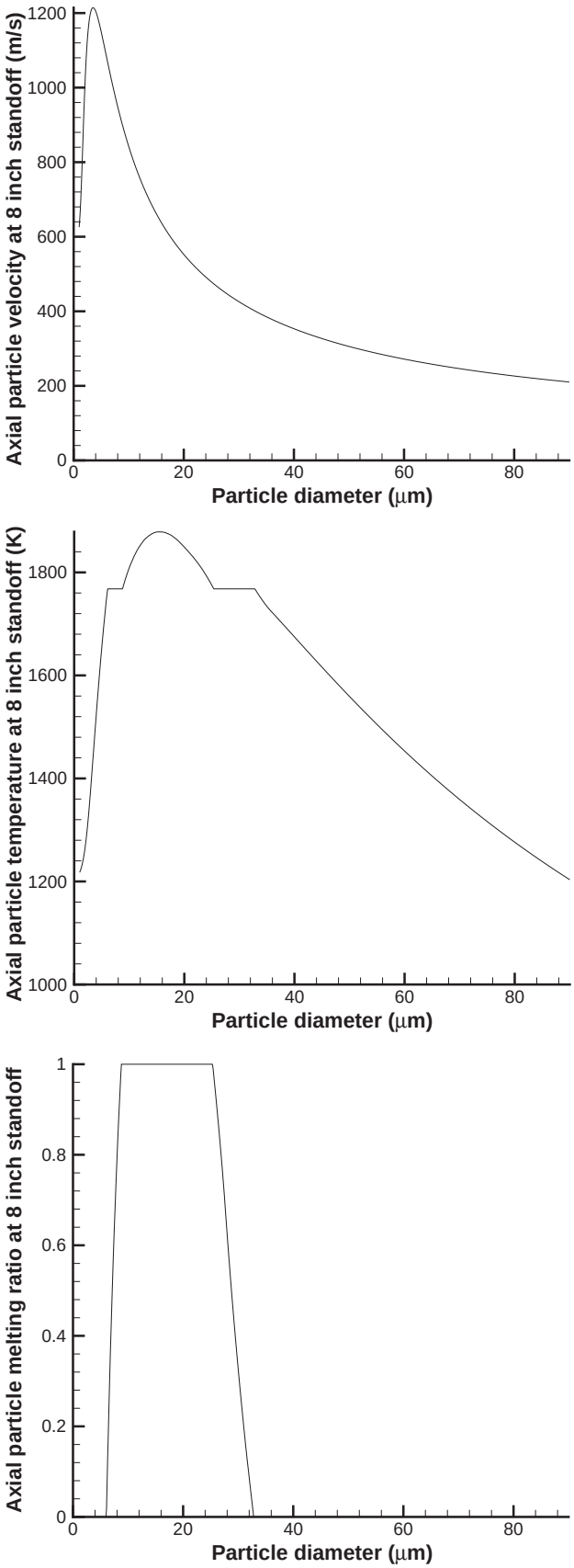

Fig. 6. Particle velocity, temperature and degree of melting at the 8 in. (0.203 m) standoff (point of impact on substrate) as a function of particle size.

state. It is worth pointing out that, although both very small particles and very big particles hit the substrate in partially molten state or even solid state, their microstructure is not the same because the former ones have been fully melted during flight.

Based on the particle behavior shown above, the coating section that is perpendicular to the substrate is simulated following the stochastic modeling procedure proposed in [8]. The coating section is discretized by a 8192 by 4096 mesh, and each cell is a square with a length of 0.1 μm. Depending on the percentage of the splat in it, a cell is either totally filled (50% or higher) or totally empty (less than 50%). The readers may refer to [8] for detailed information. Fig. 7 shows the simulated configuration of the coating sections, for particles with different molten states. The simulated section in Fig. 7(a) is formed by particles that are all fully melted (ideal case, in which the particle velocity is calculated based on the baseline operating conditions (Propylene: 176 scfh, Oxygen: 578 scfh, Air: 857 scfh and Nitrogen: 28.5 scfh), and the particle melting ratio is assumed to be one), while the one in Fig. 7(b) is formed by particles with nonuniform molten states (some particles may be partially melted or even unmelted, in which case the particle velocity, temperature and degree of melting are calculated based on the given operating conditions). The ideal lamellar structure of the thermally sprayed coating can be easily seen in Fig. 7(a). However, such a lamellar structure is disturbed by the unmelted part of the particles, as shown in Fig. 7(b). The pore distribution in the resulting coating microstructure is shown in Fig. 7(c). It can be seen that large unmelted particles affect the coating surface dramatically, thus, leading to high coating roughness. The observations clearly demonstrate that a high melting degree should be maintained in order to improve coating performance. Furthermore, it is generally acknowledged that the higher the particle velocity, the denser the coating. Therefore, the control objectives for the HVOF process considered in this work are chosen to be the regulation of the particle melting ratio and velocity at the point of impact on the substrate.

Based on the above study, a parametric analysis was carried out to study the influence of total mass flow rate and equivalence ratio on the gas properties in the internal flow field, as shown in Fig. 8. Note that since the gas properties at two positions in the internal flow field can be related by using the isentropic relationships of Eqs. (2)–(4), only the gas properties at the throat of the nozzle are listed. In Fig. 8(a), the equivalence ratio is fixed at its baseline value and the total mass flow rate varies from 0.8 to 1.2 times its baseline value. It can be seen that the pressure, density and gas momentum flux increase linearly with the total mass flow rate (slope=1.01, 0.99 and 1.01, respectively), however, the gas temperature, velocity and average molecular weight increase very little (by 4%, 1% and 1%, respectively) when the total mass flow rate increases by 200%. In

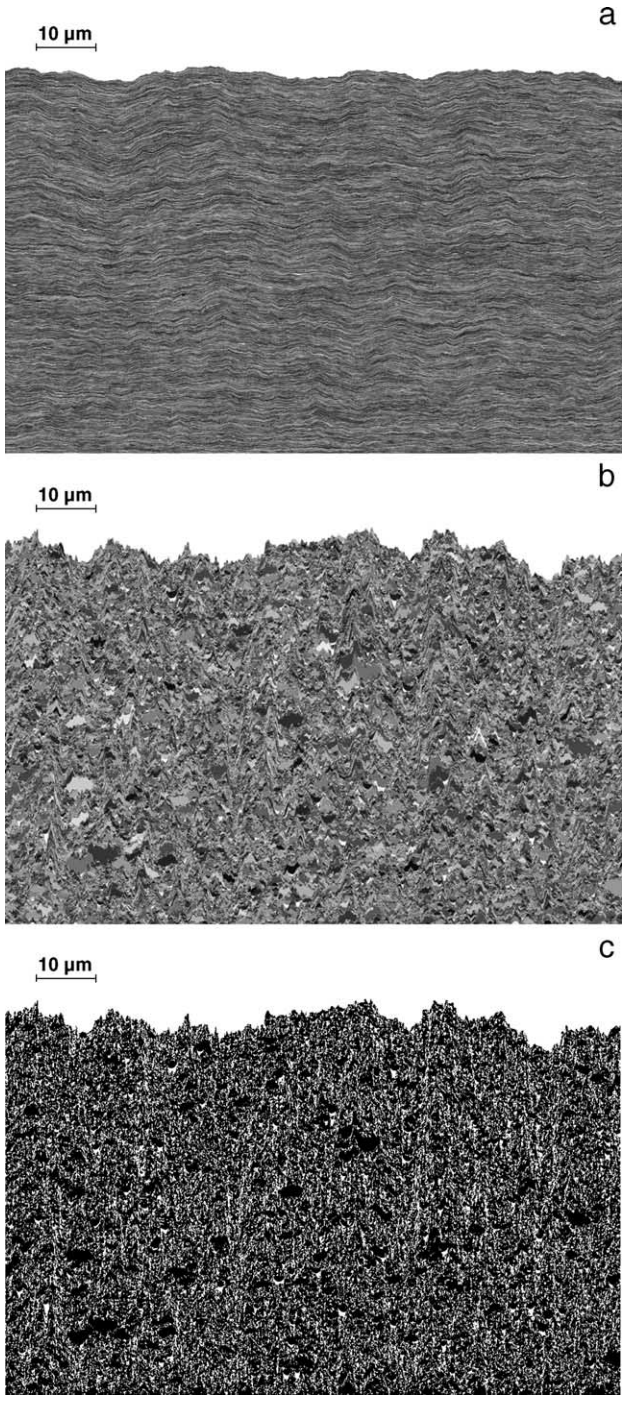

Fig. 7. Simulated microstructure of coatings made of (a) fully melted particles and (b) particles of nonuniform molten states and (c) pore distribution in the microstructure of coatings made of particles of nonuniform molten states.

Fig. 8(b), the total mass flow rate is fixed at its baseline value and the equivalence ratio varies from 0.59 to 1.86. It can be seen that the gas molecular weight decreases following a linear function and the density decreases but not so much as the molecular weight. The gas velocity, momentum flux and pressure increase constantly, following almost the same function.

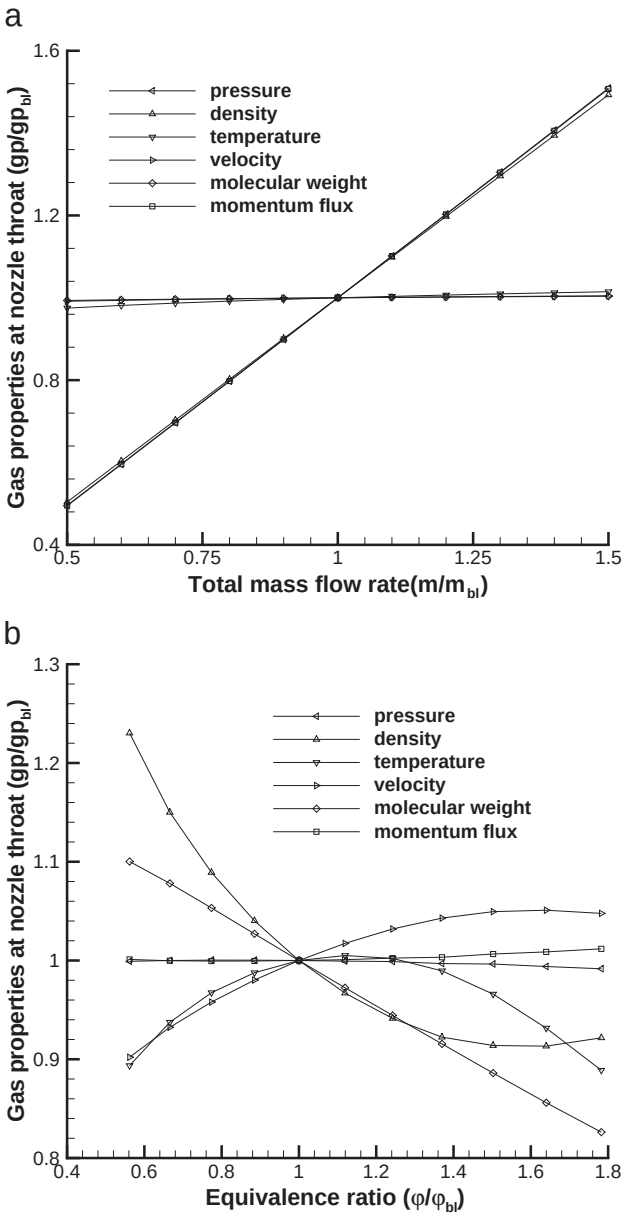

Fig. 8. Influence of total mass flow rate (a) and equivalence ratio (b) on the gas properties at the throat of the nozzle. Plotted as the ratio of total mass flow rate, equivalence ratio and gas properties to their corresponding baseline values.

The gas temperature, however, increases initially, reaching a peak value, and then decreases. Note that since the gas momentum flux ($\rho_g v_g^2$), which is approximately proportional to the drag force (when the effect of the drag coefficient is neglected), is a linear function of the chamber pressure but a weak function of the equivalence ratio ($\rho_g v_g^2 = \gamma \mathbf{M}^2 P$), and the gas temperature, is primarily dependent on the equivalence ratio but weakly dependent on the chamber pressure, it follows that the chamber pressure and equivalence ratio can be used to control the particle velocity and temperature almost independently.

5. Feedback control of HVOF process

5.1. Control problem formulation

Based on model predictions and available experimental observations, the control problem for the HVOF process is formulated as the one of regulating the volume-based averages of liquid fraction and velocity of particles at impact on the substrate (these are the variables that directly influence coating microstructure and porosity as demonstrated in the previous section, see also [8]) by manipulating the flow rates of propylene, oxygen and air at the entrance of the HVOF thermal spray gun. To develop a feedback controller that can be readily implemented in practice, the manipulation of combustion pressure and equivalence ratio is realized by adjusting the flow rate of propylene, $u_1(t)$, oxygen, $u_2(t)$, and air, $u_3(t)$. Owing to the almost decoupled nature of the manipulated input/controlled output pairs, two proportional integral (PI) controllers are used to regulate the process. Specifically, the controllers have the following form:

$$\dot{\zeta}_i = y_{\mathrm{sp}_i} - y_i,\ \zeta_I(0) = 0,\ i = 1,2$$

$$u'_I = K_{\mathrm{c}_i}\left[\left(y_{\mathrm{sp}_I} - y_i\right) + \frac{1}{\tau_{\mathrm{c}_i}}\zeta_i\right] + u'_{0_i},\ i = 1,2$$

$$\{u_1, u_2, u_3\} = f\left(u'_1, u'_2, w\right) \tag{23}$$

where y_{sp_i} is the desired set-point value and y_i is the value of the output obtained from the measurement system (y_1 is the volume-based average of particle velocity and y_2 is the volume-based average of melting ratio), u'_1 is the combustion pressure and u'_2 is the equivalence ratio. K_{c_i} is the proportional gain and τ_{c_i} is the integral time constant. The third equation makes use of the process model. To keep the problem simple, the ratio of air to oxygen (or w) is fixed. Note that the relationship between the gas temperature and the equivalence ratio is not monotonic. Beyond the optimal equivalence ratio (about 1.2), the gas temperature decreases as the equivalence ratio increases. Therefore, K_{c_2} should be replaced by $-K_{\mathrm{c}_2}$ when the initial equivalence ratio is above this value. An important assumption is that the time scale of gas dynamics is much smaller than the particle inflight time. This assumption is generally true, especially for large particles, as one can see from Fig. 5. The consequence of this assumption is that the gas dynamics can be considered to be at steady state.

Particle coagulation in the HVOF thermal spray process has not been reported in the literature, which may be explained by the following argument. The average distance between individual particles in the HVOF thermal spray process can be estimated based on the analysis of Crowe et al. [43]. Specifically,

$$\frac{L_{\mathrm{d}}}{d_{\mathrm{p}}} = \left[\frac{\pi}{6}\frac{1+\kappa}{\kappa}\right]^{1/3} \tag{24}$$

where L_d is the distance between two particles and κ is the ratio of particle loading to particle/gas density ratio. Usually the particle loading is about 4%, the density ratio is about 10^{3-4}, therefore L_d/d_p is about 20–50, which implies that the individual powder particles can be considered isolated from each other. Therefore, in this work, we assume that particle coagulation is negligible and the powder size distribution does not change during flight. To calculate the volume-based average of particle properties, a lognormal distribution function is used [13,14,21,22]. In this work, the average powder properties ($\overline{PP}$) are calculated based on particle volume:

$$\overline{PP} = \frac{\int_{d_{lb}}^{d_{ub}} \frac{1}{6}\pi d_p^3 PP(d_p) f(d_p) d(d_p)}{\int_{d_{lb}}^{d_{ub}} \frac{1}{6}\pi d_p^3 f(d_p) d(d_p)} \quad (25)$$

because larger particles have a stronger influence on coating properties than smaller ones. In our computer simulations, we integrate the numerator and denominator from a lower bound (d_{lb}) to an upper bound (d_{ub}) in order to capture more than 99 wt.% of all the particles in the spray.

Regarding the practical implementation of the proposed control system on the HVOF thermal spray process, we note that the chamber pressure and the equivalence ratio can be readily manipulated in real-time by adjusting the mass flow rates of fuel, oxygen and air. The velocity and temperature of individual particles can be measured experimentally using non-intrusive optical techniques, for example, Laser Doppler Velocimetry [44], Particle Imaging Velocimetry [45,46], Two Color Pyrometry [47–49], etc. However, it is not possible to directly measure the degree of melting of individual particles and consequently, the average degree of melting of the entire particle size distribution. To overcome this limitation, one needs to use an estimation scheme based on the modeling equations that describe the evolution of particle temperature, velocity and degree of particle melting coupled with the available gas phase measurements to estimate average particle melting ratio at the point of impact on the substrate. The estimates obtained by this model can be further improved through comparison with the particle temperature measurements at various locations across the free jet. In the simulation section, we have included a closed-loop simulation in the presence of measurement errors to evaluate the effect of such errors in closed-loop performance; the detailed development of an estimation scheme for particle melting ratio is the subject of future work. The controller then obtains information from the measurement system, and makes decisions, which are sent to the controlled valves (total flow of gases to the process and oxygen/fuel ratio), to adjust the manipulated input variables until the deviation of the controlled outputs from their corresponding set-point values falls within a tolerable region. One of the great advantages of feedback control is that it can compensate for the effect of disturbances in the process operating conditions.

Table 5
Parameters used in the closed-loop simulation

K_{c_1}	1×10^{-2}
K_{c_2}	0.1
τ_1	5×10^{-2}
τ_2	5×10^{-2}

Table 6
Thermophysical properties of WC–12%Co particles

ρ_p (kg/m^3)	14320
c_{p_p} (J/kg K)	295.4
T_m[a] (K)	1768
ΔH_m (J/kg)	4.2×10^5
ε	0.4
d_{10} (μm)	5
d_{50} (μm)	15
d_{90} (μm)	45

[a] Melting point of Cobalt.

5.2. Closed-loop simulations

In this subsection, simulation runs of the closed-loop system are presented. The outputs $y_1(t)$ and $y_2(t)$ are computed by averaging the individual particle velocity and liquid fraction data obtained from the process model. To account for the powder size distribution, we first fit a lognormal distribution and calculate the size range in order to capture more than 99 wt.% of all the particles. We then divide this size range into 100 intervals to perform the integration. Further increase on the number of discretization intervals did not change the accuracy of the computed results [13,14,22]. This requires solving simultaneously 400 ordinary differential equations for each process simulation. The parameters used in the closed-loop system simulations are shown in Table 5 and the particle thermophysical properties are given in Table 6.

Several simulation runs of the process model under the feedback controller were performed to evaluate the ability of the controller to: a) regulate the velocity and melting ratio of particles at the point of impact on substrate to desired set-point values, b) attenuate the effect of disturbances on process operating conditions and c) compensate for the effect of measurement errors. The first simulation studies the behavior of the closed-loop system in the presence of changes in the set-point. Initially, the process is assumed to operate under the baseline conditions, and at time $t=10$ s, the average particle velocity set-point value increases by 5% and the average particle melting set-point value increases by 5%. Fig. 9 shows how the controlled outputs and manipulated inputs evolve in the case of requesting such changes in the set-point values. The feedback controller drives the controlled outputs to the new set points in about 5 s, which means that the controller is quite effective and validates the feasibility of implementation of real-time feedback control on the HVOF process.

To test the robustness of the proposed control problem formulation and of the feedback controller, the problem of

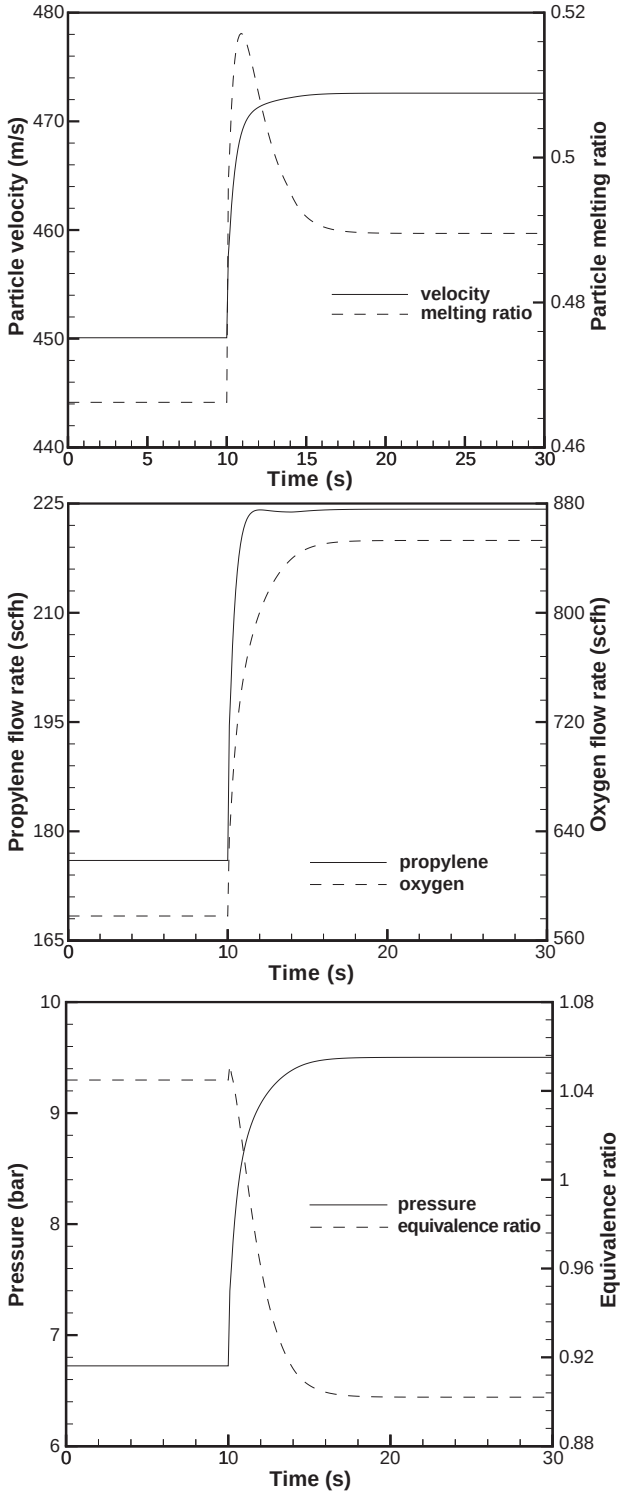

Fig. 9. Profiles of controlled outputs (average particle velocity and melting ratio), manipulated inputs (flow rate of propylene, oxygen and air) and pressure and equivalence ratio under the request of 5% increase in particle velocity and 5% increase in melting ratio.

controlling the HVOF process in the presence of disturbances was studied. Figs. 10 and 11 show the controlled output and manipulated input profiles in the presence of disturbances (10% increase and 10% decrease, respectively) in the spray distance which occurs at $t=10$ s. Without control, the particle velocity in both cases drops instantaneously. The reason is that the particles are usually accelerated first and then decelerated in the external field, and therefore there is

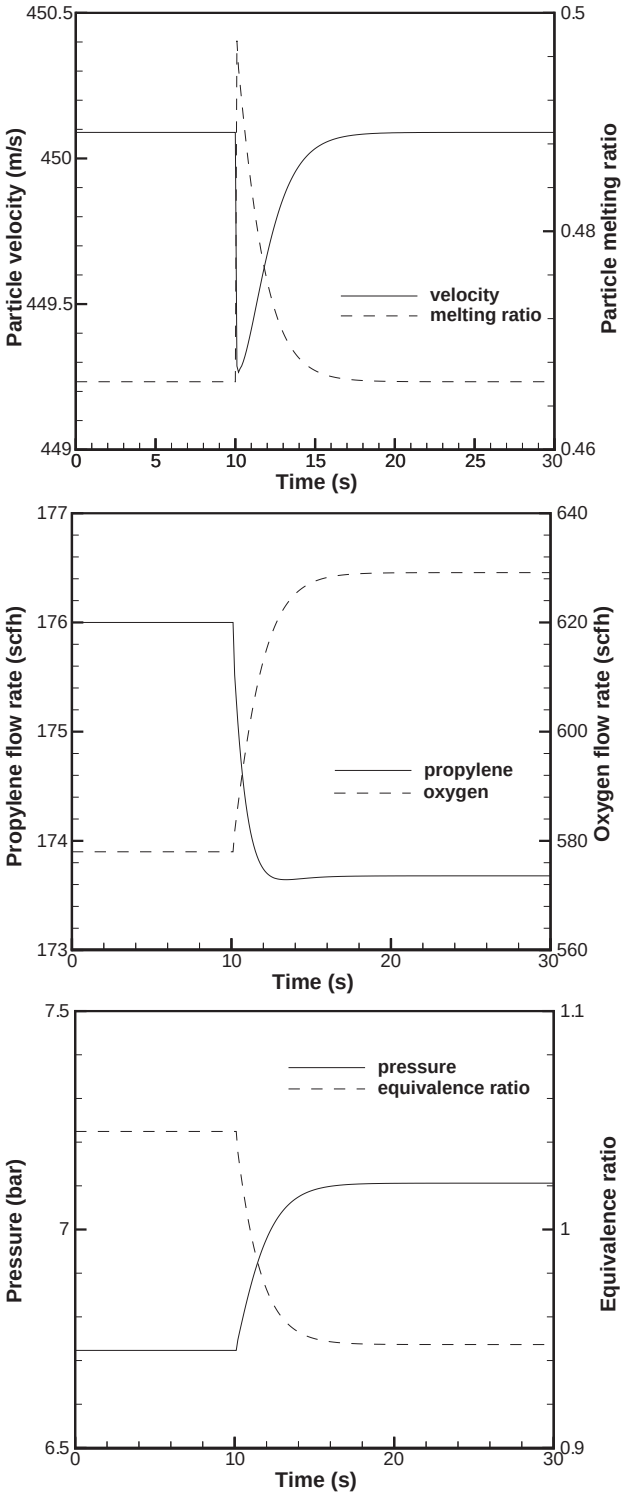

Fig. 10. Profiles of controlled outputs (average particle velocity and melting ratio), manipulated inputs (flow rate of propylene, oxygen and air) and pressure and equivalence ratio in the presence of 10% decrease in spray distance.

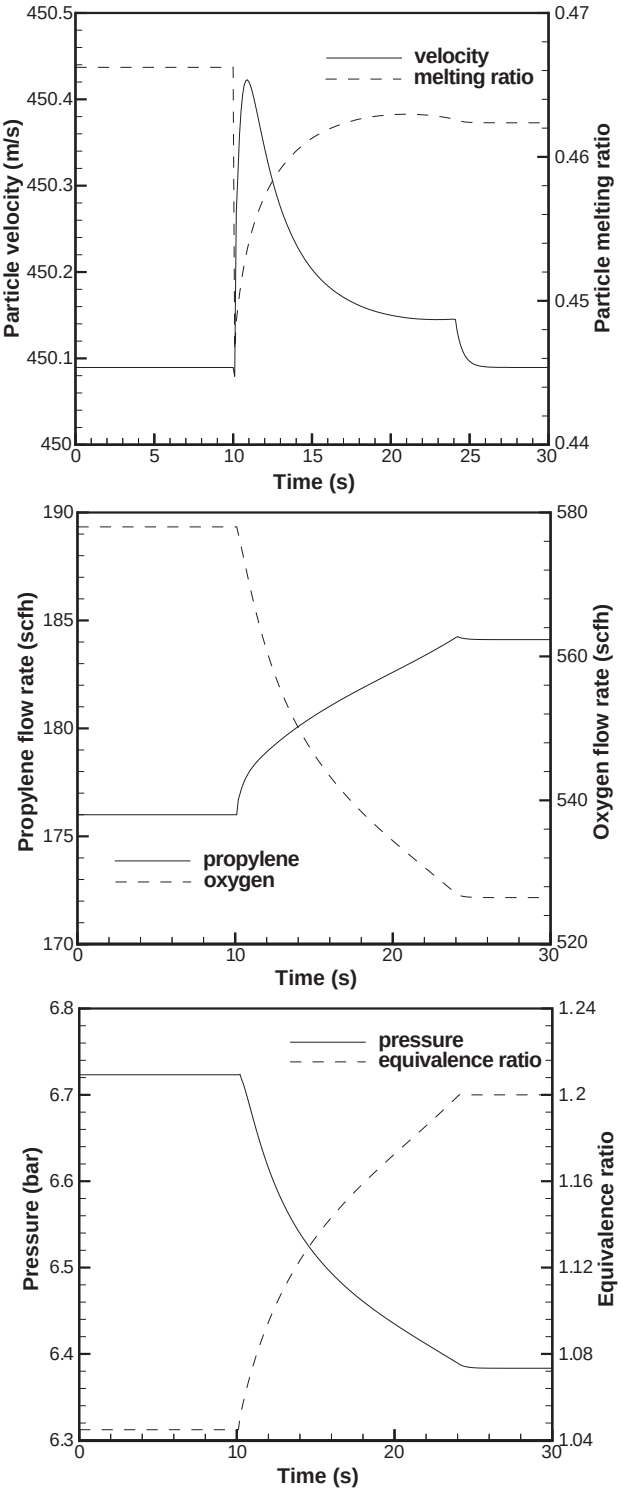

Fig. 11. Profiles of controlled outputs (average particle velocity and melting ratio), manipulated inputs (flow rate of propylene, oxygen and air) and pressure and equivalence ratio in the presence of 10% increase in spray distance.

an optimal spray distance. Nevertheless, the disturbances in spray distance do not have a significant effect on particle velocity because the velocity profile of particles is almost flat as they reach the gas velocity. However, the melting

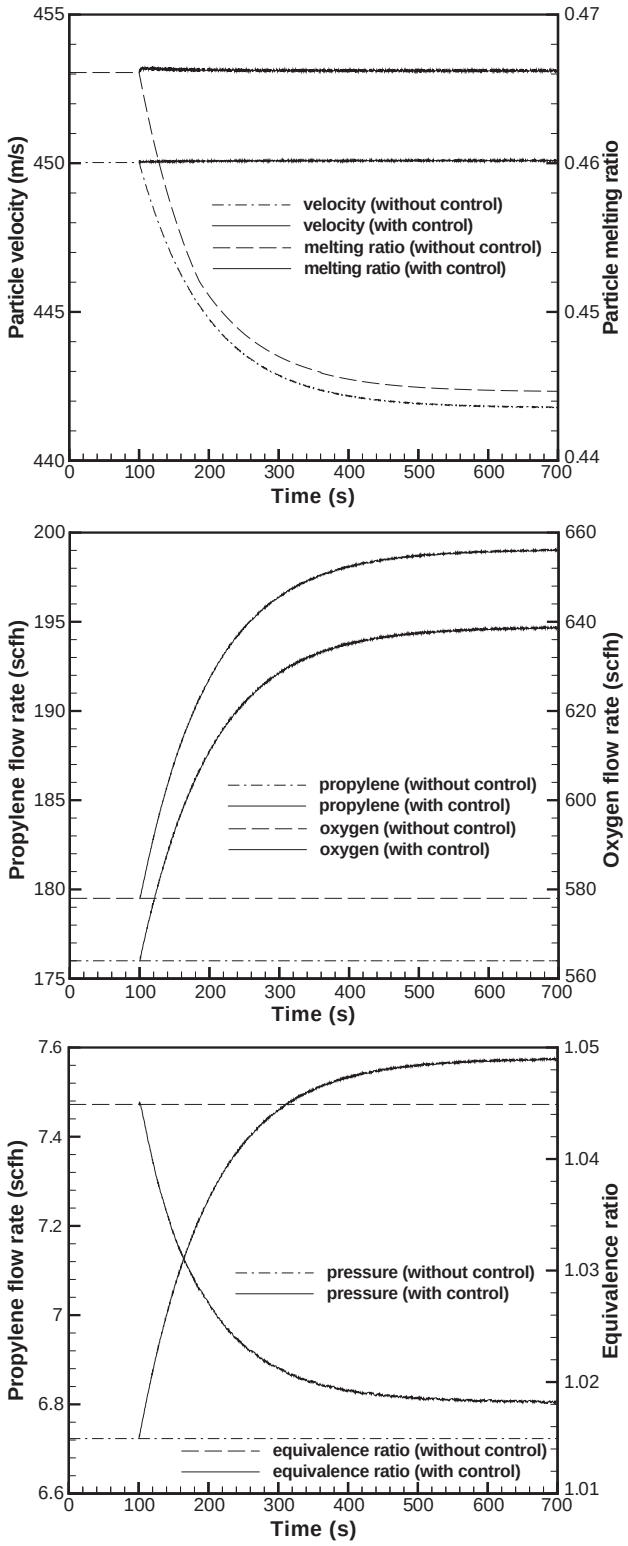

Fig. 12. Profiles of controlled outputs (average particle velocity and melting ratio), manipulated inputs (flow rate of propylene, oxygen and air) and pressure and equivalence ratio in the presence of variation in powder size distribution.

ratio of particles at the point of impact on substrate decreases when the spray distance increases, and increases when the spray distance decreases. This can be explained by the change of particle residence time in the gas flame. Such variations in the molten state of the particle may have a detrimental effect on the coating microstructure and properties. Under feedback control, the manipulated inputs drive the process outputs to their original steady state values in 10 s for the first case. However, for the second case, although the particle velocity reaches its desired set-point value eventually, the desired particle melting ratio is not achieved. This is because the initial operating condition is very close to the optimal one ($\varphi \approx 1.2$) and the particle temperature cannot be increased further.

Another source of disturbance to the process operation, especially in an industrial environment, is the variation of the size distribution of the powder during the operation of the HVOF process. This may have a significant influence on the particle velocity and particle temperature at the point of impact on the substrate based on the analysis of the previous sections. In the following simulation, it is assumed that the process is at steady-state in the first 100 s and then the powder size distribution changes gradually (specifically, in the following calculation, the characteristic sizes describing lognormal distribution, d_{10}, d_{50}, d_{90} increases according to the expression $d_p = d_{p_0}[1+0.03(1-e^{-t/100})]$). Fig. 12 shows the controlled output and the manipulated input profiles in the presence of such a variation in the powder size distribution. Under feedback control, both particle velocity and liquid fraction fluctuate in a very narrow range around the desired set-point values. When no control is used, in which case the flow rate of each stream is kept constant, both the velocity and the melting ratio of particles decrease with time, which may have an undesirable effect on the resulting coating properties.

To demonstrate that the proposed formulation of the control problem is robust with respect to measurement errors, we implemented the developed control system on the process model under the request of 5% increase in average particle melting ratio set-point value and 5% increase in the average particle velocity set-point value at time $t=10$ s but assuming that there are errors in the values of average velocity and degree of melting used in the controller. In the closed-loop simulation, we assume that the estimation errors follow an exponentially-decaying function with an initial error of 10%. The corresponding controlled and manipulated input variables are given in Fig. 13. The results show that the desired control objective of 5% change in the set-point values is eventually achieved (compare the controlled output profiles of Figs. 9 and 13); this demonstrates that the proposed formulation of the control problem is robust with respect to measurement errors. The readers may refer to [50] for model-based estimation and control of particle velocity and melting in the HVOF thermal spray process.

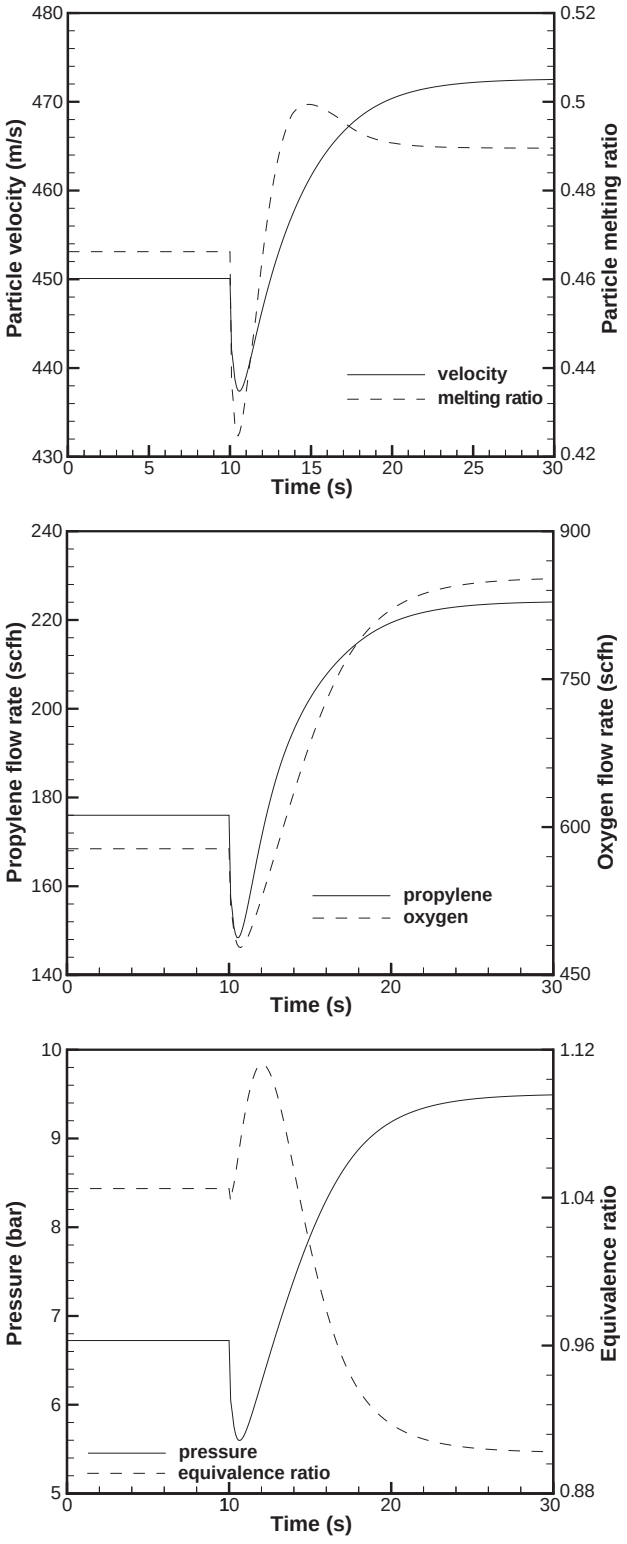

Fig. 13. Profiles of controlled outputs (average particle velocity and melting ratio), manipulated inputs (flow rate of propylene, oxygen and air) and pressure and equivalence ratio under the request of 5% increase in particle velocity and 5% increase in melting ratio—closed-loop simulation in the presence of measurement error.

In summary, the closed-loop system simulations demonstrated that the proposed controller attenuates the effect of disturbances and drives the controlled outputs to the desired set-point values within a very short time and is also robust with respect to measurement errors.

6. Conclusion

This work focused on modeling and control of an HVOF thermal spray process used to process WC-Co coatings. The simulation results, based on a fundamental process model, demonstrated that the particle-melting degree and the particle velocity strongly influence coating microstructure formation and can be adjusted by the equivalence ratio and the chamber pressure. The control problem was formulated as the one of regulating volume-based averages of particle velocity and melting degree at the point of impact on substrate by manipulating the gas flow rate of air, oxygen, and fuel at the entrance of the thermal spray gun. A feedback control system was developed and applied to the detailed mathematical model of the process. Closed-loop simulations demonstrated that the proposed feedback controller is effective in driving the controlled outputs to the desired set-point values and attenuates the effect of various external disturbances in the operating environment.

Nomenclature

A	cross area perpendicular to the flow direction (m^2)
A_p	projected area of a particle on the plane perpendicular to the flow (m^2)
A'_p	surface area of particles (m^2)
A_s	area of the splat (m^2)
Bi	Biot number
c_p	heat capacity at constant pressure (J/mol K for gas or J/kg K for particle)
C_D	drag coefficient
d_p	particle diameter (m)
D	diameter of the gun barrel (m)
D_s	diameter of splat (m)
f_p	melting degree of particles
gp	gas property
h	heat transfer coefficient (W/m^2 K)
H_s	height of the splat (m^2)
J	heat transfer rate (W)
L_d	average distance between particles (m)
K_c	proportional gain
m	mass (kg)
M	Mach number
P	pressure (Pa)
Pe	Peclet number
PP	particle properties
Pr	Prandtl number
R	gas constant (8.314 J/mol K)
Re	Reynolds number
S_h	source term of heat transfer (W)
T	temperature (K)
t	time (s)
u	manipulated input
w	coefficients of nitrogen from air in Eq. (1)
We	Weber number
v	velocity (m/s)
x	axial distance (m)
y	controlled output
z	coefficients of carrier in Eq. (1)

Greek letters

α, β	factors used in Eq. (6)
η	viscosity (kg/m/s)
γ	specific heat ratio
λ	thermal conductivity (J/m^2 K)
κ	ratio of particle loading to particle/gas density ratio
μ	Mean
ρ	density (kg/m^3)
σ	Stephan–Boltzmann constant (5.67×10^{-8} W/m^2 K^4)
σ^2	Variation
τ_c	integral time constant
φ	equivalence ratio
ξ	flattening ratio
ξ_i	stoichiometric coefficient (mol/kg)
ζ	Error

Superscripts and subscripts

0	initial value
a	ambient condition
cov	Convection
e	exit condition
g	properties related to gas
m	Melting
p	properties related to particles
pr	Products
rad	Radiation
sp	specified value
T	Total
t	Throat
–	normalized variable
·	time derivative

Acknowledgement

Financial support from a 2001 ONR Young Investigator Award is gratefully acknowledged.

References

[1] D. Cheng, G. Trapaga, J.W. McKelliget, E.J. Lavernia, Mathematical modelling of high velocity oxygen fuel thermal spraying of nanocrystalline materials: an overview, Model. Simul. Mater. Sci. Eng. 11 (2003) R1–R31.

[2] D. Cheng, Q. Xu, G. Trapaga, E.J. Lavernia, A numerical study of high-velocity oxygen fuel thermal spraying process: Part I. Gas phase dynamics, Metall. Mater. Trans., A Phys. Metall. Mater. Sci. 32 (2001) 1609–1620.
[3] D. Cheng, Q. Xu, G. Trapaga, E.J. Lavernia, The effect of particle size and morphology on the in-flight behavior of particles during high-velocity oxyfuel thermal spraying, Metall. Mater. Trans., B 32 (2001) 525–535.
[4] H. Liu, E.J. Lavernia, R.H. Rangel, Modeling of molten droplet impingement on a nonflat surface, Acta Metall. Mater. 43 (1995) 2053–2072.
[5] M. Bussmann, J. Mostaghimi, S. Chandra, On a three-dimensional volume tracking model of droplet impact, Phys. Fluids 11 (1999) 1406–1417.
[6] W.D. Cai, E.J. Lavernia, Modeling of porosity during spray forming, Mater. Sci. Eng., A Struct. Mater.: Prop. Microstruct. Process. 226 (1997) 8–12.
[7] R. Ghafouri-Azar, J. Mostaghimi, S. Chandra, M. Charmchi, A stochastic model to simulate the formation of a thermal spray coating, J. Therm. Spray Technol. 12 (2003) 53–69.
[8] D. Shi, M. Li, P.D. Christofides, Diamond jet hybrid HVOF thermal spray: rule-based modeling of coating microstructure, Ind. Eng. Chem. Res. 43 (2004) 3653–3665.
[9] S. Annavarapu, D. Apelian, A. Lawley, Spray casting of steel strip: process analysis, Metall. Trans., A, Phys. Metall. Mater. Sci. 21 (1990) 3237–3256.
[10] P. Marthur, S. Annavarapu, D. Apelian, A. Lawley, Spray casting: an integral model for process understanding and control, Mater. Sci. Eng., A Struct. Mater.: Prop. Microstruct. Process. 142 (1991) 261–276.
[11] J.R. Fincke, W.D. Swank, R.L. Bewley, D.C. Haggard, M. Gevelber, D. Wroblewski, Diagnostics and control in the thermal spray process, Surf. Coat. Technol. 146–147 (2001) 537–543.
[12] C. Moreau, L. Leblanc, Optimization and process control for high performance thermal spray coatings, Key Eng. Mater. 197 (2001) 27–57.
[13] M. Li, P.D. Christofides, Modeling and analysis of HVOF thermal spray process accounting for powder size distribution, Chem. Eng. Sci. 58 (2003) 849–857.
[14] M. Li, P.D. Christofides, Feedback control of HVOF thermal spray process accounting for powder size distribution, J. Therm. Spray Technol. 13 (2004) 108–120.
[15] T. Chiu, P.D. Christofides, Nonlinear control of particulate processes, AIChE J. 45 (1999) 1279–1297.
[16] T. Chiu, P.D. Christofides, Robust control of particulate processes using uncertain population balances, AIChE J. 46 (2000) 266–280.
[17] N.H. El-Farra, T. Chiu, P.D. Christofides, Analysis and control of particulate processes with input constraints, AIChE J. 47 (2001) 1849–1865.
[18] A. Kalani, P.D. Christofides, Nonlinear control of spatially-inhomogeneous aerosol processes, Chem. Eng. Sci. 54 (1999) 2669–2678.
[19] A. Kalani, P.D. Christofides, Modeling and control of a titania aerosol reactor, Aerosol Sci. Tech. 32 (2000) 369–391.
[20] A. Kalani, P.D. Christofides, Simulation, estimation and control of size distribution in aerosol processes with simultaneous reaction, nucleation, condensation and coagulation, Comput. Chem. Eng. 26 (2002) 1153–1169.
[21] P.D. Christofides, Model-based control of particulate processes, Kluwer Academic, Particle Technology Series, Netherlands, 2002.
[22] M. Li, D. Shi, P.D. Christofides, Diamond jet hybrid HVOF thermal spray: gas-phase and particle behavior modeling and feedback control design, Ind. Eng. Chem. Res. 43 (2004) 3632–3652.
[23] X. Yang, S. Eidelman, Numerical analysis of a high-velocity oxygen-fuel thermal spray system, J. Therm. Spray Technol. 5 (1996) 175–184.
[24] D. Cheng, G. Trapaga, J.W. McKelliget, E.J. Lavernia, Mathematical modeling of high velocity oxygen fuel thermal spraying: an overview, Key Eng. Mater. 97 (2001) 1–25.
[25] W.D. Swank, J.R. Fincke, D.C. Haggard, G. Irons, HVOF gas flow field characteristics. In: Proceedings of the 7th National Thermal Spray Conference, 1994, pp. 313–318.
[26] A. Dolatabadi, J. Mostaghimi, V. Pershin, Effect of a cylindrical shroud on particle conditions in high velocity oxy-fuel spray process, J. Mater. Process. Technol. 137 (2003) 214–224.
[27] V. Gourlaouen, E. Verna, P. Beaubien, Influence of flame parameters on stainless steel coatings properties. Thermal Spray: Surface Engineering via Applied Research, Proceedings of the International Thermal Spray Conference, ASM International, Montreal, QC, Canada, 2000, pp. 487–493.
[28] G.D. Power, E.B. Smith, T.J. Barber, L.M. Chiappetta, Analysis of a combustion (HVOF) spray deposition gun, Report 91-8, United Technologies Research Center, East Hartford, Connecticut, USA, 1991.
[29] S. Gordon, B.J. McBride, Computer Program for Calculation of Complex Chemical Equilibrium Compositions and Applications, NASA Reference Publication, vol. 1311, Lewis Research Center, Cleveland, Ohio, USA, 1994.
[30] L.Y. Jiang, J.P. Sislian, LDV measurements of mean velocity components and turbulence intensities in supersonic high-temperature exhaust plumes, AIAA Pap. (1993) 93–3069.
[31] L.Y. Jiang, J.P. Sislian, Velocity and density measurements in supersonic high-temperature exhaust plumes, AIAA J. 36 (1998) 1216–1222.
[32] N.T. Lagen, J.M. Seiner, Evaluation of Water Cooled Supersonic Temperature and Pressure Probes for Application to 2000 F Flows, NASA Technical Memorandum, vol. 102612, Langley Research Center, 1990.
[33] W.D. Swank, J.R. Fincke, D.C. Haggard, G. Irons, R. Bullock, HVOF particle flow field characteristics, Proceedings of the 7th National Thermal Spray Conference, 1994, pp. 319–324. Boston, MA.
[34] H.H. Tawfik, F. Zimmerman, Mathematical modeling of the gas and powder flow in HVOF systems, J. Therm. Spray Technol. 6 (1997) 345–352.
[35] R.B. Bird, W.E. Stewart, E.N. Lightfoot, Transport Phenomena, John Wiley Sons, New York, USA, 1960.
[36] V.V. Sobolev, J.M. Guilemany, J.C. Garmier, J.A. Calero, Modelling of particle movement and thermal behavior during high velocity oxy-fuel spraying, Surf. Coat. Technol. 63 (1994) 181–187.
[37] E.L. Crow, K. Shimizu, Lognormal Distributions: Theory and Applications, Marcel Dekker, New York, USA, 1988.
[38] M.L. Lau, H.G. Jiang, W. Nuchter, E.J. Lavernia, Thermal spraying of nanocrystalline Ni coatings, Phys. Status Solidi A, Appl. Res. 166 (1998) 257–268.
[39] J. Madejski, Solidification of droplets on a cold surface, Int. J. Heat Mass Transfer 19 (1976) 1009–1013.
[40] D. Mills, Personal communication, Sulzer Metco, 2003.
[41] M. Li, P.D. Christofides, Multi-scale modeling and analysis of an industrial HVOF thermal spray process. Chem. Eng. Sci. 60 (2005) 3649–3669.
[42] C.J. Geankoplis, Transport Processes and Unit Operations, 3rd ed., Prentice-Hall, New Jersey, USA, 1993.
[43] C.T. Crowe, M. Sommerfeld, Y. Tsuji, Multiphase Flows with Droplets and Particles, CRC Press, Boca Raton, FL, USA, 1997.
[44] J.R. Fincke, W.D. Swank, C.L. Jeffrey, Simultaneous measurement of particle size, velocity and temperature in thermal plasmas, IEEE Trans. Plasma Sci. 18 (1990) 948–957.
[45] R. Knight, R.W. Smith, Z. Xiao, Particle velocity measurements in HVOF and APS systems, Thermal Spray Industrial Applications. Proceedings of 7th National Thermal Spray Conference, 1994, pp. 331–336.
[46] I. Thomson, V. Pershin, J. Mostaghimi, S. Chandra, Experimental testing of a curvilinear gas shroud nozzle for improved plasma spraying, Plasma Chem. Plasma Process. 21 (2001) 65–82.

[47] W.D. Swank, J.R. Fincke, D.C. Haggard, A particle temperature sensor for monitoring and control of the thermal spray process, Proceedings of the 8th National Thermal Spray Conference, 1995, pp. 111–116. Houston, TX.
[48] T.C. Hanson, C.M. Hackett, G.S. Settles, Independent control of HVOF particle velocity and temperature, J. Therm. Spray Technol. 11 (2002) 75–85.
[49] J.R. Fincke, D.C. Haggard, W.D. Swank, Particle temperature measurement in the thermal spray process, J. Therm. Spray Technol. 10 (2001) 255–266.
[50] M. Li, D. Shi, P.D. Christofides, Model-based estimation and control of particle velocity and melting in HVOF thermal spray, Chem. Eng. Sci. 59 (2004) 5647–5656.